

Global room-temperature superconductivity in graphite

Y. V. Kopelevich¹, J. H. S. Torres¹, R. Ricardo da Silva¹, and V. M. Vinokur²

¹Universidade Estadual de Campinas-UNICAMP, Instituto de Física “Gleb Wataghin”, R. Sergio Buarque de Holanda 777, 13083-859 Campinas, Brazil

²Terra Quantum AG, CH-9400 Rorschach, Switzerland

Abstract

We report unambiguous experimental evidence for the global room-temperature superconductivity in cleaved highly oriented pyrolytic graphite (HOPG) carrying dense arrays of nearly parallel line defects (LD) at its surface. Multiterminal resistance $R(T, B)$ and current-voltage characteristics $I-V(T, B)$ are measured in the temperature interval $4.5 \text{ K} \leq T \leq 300 \text{ K}$ and magnetic fields $0 \leq B \leq 9 \text{ T}$ applied perpendicular to basal graphitic planes. We find that the superconducting critical current $I_c(T, B)$ is governed by the normal state resistance $R_N(T, B)$, so that $I_c(T, B) \sim 1/R_N(T, B)$ for all measuring temperatures and magnetic fields, which is consistently understood in terms of “granular” superconductivity emerging in the LD. We discuss the possible stabilizing effect of the underlying Bernal graphite on the inter-grain superconducting phase coherence, that brings the zero-resistance transition temperature T_C close to the electron-electron pairing temperature $T_C^0 > 300 \text{ K}$.

The phenomenon of superconductivity (SC) has been discovered by Kamerlingh Onnes in 1911 [1]. The first superconducting material was mercury (Hg) with the superconducting transition temperature $T_C = 4.2 \text{ K}$. Ever since, one of the major directions in the field of superconductivity has been a tireless search for materials with the highest possible T_C . The discovery of high-temperature superconductivity (HTSC) in the Ba-La-Cu-O cuprates with $T_C \approx 30 \text{ K}$ [2] and Y-Ba-Cu-O with T_C as high as 93 K [3] marked a breakthrough in this search and brought a hope for fast coming of the room temperature superconductivity (RTSC). So far, the highest $T_C = 135 \text{ K}$ under the ambient pressure showed the mercury-based cuprate $\text{HgBa}_2\text{Ca}_2\text{Cu}_3\text{O}_9$ [4] which then was raised up to 164 K under the pressure of 30 GPa [5]. Outside the cuprate family, the highest $T_C = 33 \text{ K}$ at the equilibrium was observed in the alkali-doped fullerenes $\text{Cs}_x\text{Rb}_y\text{C}_{60}$ [6] and MgB_2 with $T_C = 39 \text{ K}$ [7]. Very recently, a zero-resistance state near the room temperature has been reported in various hydride systems under the pressure $P > 200 \text{ GPa}$ [8]. Graphite is yet another promising material taking part in a race for the RTSC. First, the bulk superconductivity was found in the alkali-metal graphite intercalation compound (GIC) C_8K with $T_C = 0.15 \text{ K}$ [9]. Then, after 40 years of the research, C_6Yb and C_6Ca raised it to $T_C = 6.5 \text{ K}$ and $T_C = 11.5 \text{ K}$ respectively [10, 11]. Decades ago, Antonowicz has measured Josephson-type oscillations and Shapiro-like steps in current-voltage ($I-V$) characteristics at $T = 300 \text{ K}$ in Al-AC-Al sandwiches (AC = amorphous carbon) [12, 13]. Various experimental groups have also reported localized superconductivity in graphite at temperatures as high as 300 K [14-18]. Both sulfur (S)-doped AC [19] and S-doped polycrystalline graphite [15, 16, 20] revealed the local superconductivity with nearly the same highest T_C of about 38 K . Because the AC consists of the curved graphene and/or the fullerene-like fragments [21], one can justly assume that similar structural defects in graphite may be

responsible for the occurrence of high-temperature localized superconducting regions. However, so far, all the efforts to achieve a global superconductivity at elevated temperatures in graphite have been failing [22-24]. In the present work we report the unambiguous experimental evidence for the global (zero-resistance state) RTSC in cleaved, by means of “Scotch Tape”, highly oriented pyrolytic graphite (HOPG) that possesses dense arrays of nearly parallel line defects (LD) [25].

The multi-terminal basal-plane resistance $R_b(T, B, I)$ measurements are taken on the freshly cleaved HOPG sample with the dimensions of $l \cdot w \cdot t = 5 \cdot 4 \cdot 0.5 \text{ mm}^3$, obtained from the Union Carbide Co., using Janis 9 T-magnet He-cryostat, Keithley 6220 Precision Current Source, Keithley 2182A Nanovoltmeter, and Lake Shore 340 Temperature Controller. The studied samples possess the out-of-plane/basal-plane resistivity ratio $\rho_c/\rho_b \approx 3 \cdot 10^4$ at $T = 300 \text{ K}$ and $B = 0$, with $\rho_b = 5 \text{ } \mu\Omega\cdot\text{cm}$. The X-ray diffraction (Θ - 2Θ) spectra of the virgin HOPG samples demonstrate a characteristic hexagonal graphite structure with no signatures of other phases. The obtained crystal lattice parameters are $a = 2.48 \text{ } \text{Å}$ and $c = 6.71 \text{ } \text{Å}$. The high degree of crystallites orientation along the hexagonal c -axis is confirmed by the X-ray rocking curve measurements with the full width at half maximum (FWHM) = 0.3° . The measurements are performed in the temperature interval $4.5 \text{ K} \leq T \leq 300 \text{ K}$, applied magnetic fields $0 \leq B \leq 9 \text{ T}$, and the dc electric current $I \geq 5 \text{ } \mu\text{A}$. In experiments we use the line-electrode geometry [26 -28] to measure the in-plane resistance in both local and “non-local” configurations. Eleven silver epoxy electrodes with the contact resistance $R_C \approx 1 \text{ } \Omega$, oriented perpendicular to the wrinkles, are patterned on one of the main surfaces of the sample with the separation distance $d = 0.2 \text{ mm}$, as shown in Fig. 1. In the course of measurements, the dc current is applied either between the current leads 1 and 11 (I_{1-11}), or 1 and 4 (I_{1-4}). In the first configuration, we measure the voltages $V_{23} \dots V_{10-11}$ in the current-applied region (“local” voltages). In the second case, the voltage drops were measured simultaneously in both the applied current part of the crystal V_{23} and outside that region ($V_{56} \dots V_{10-11}$) (“non-local” configuration). Here we report the results obtained for I_{1-11} - V_{9-10} configuration. All the transport measurements are performed for the $B \parallel c$ - axis.

Figure 2(a, b) presents the I-V characteristics measured at $T = 300 \text{ K}$. The data demonstrate the zero-resistance state below the magnetic-field-dependent critical current $I_c(B)$ which is decreasing function of the field. The obtained I-V curves demonstrate the characteristic features known for low-dimensional superconductors. Firstly, the “excess voltage” peaks seen just above the $I_c(B)$ and before the Ohmic regime sets in at $I > I_N$, see Fig. 2b, are similar to that measured in one (1D) - or two (2D) -dimensional superconducting constrictions, attributed to the charge imbalance and/or presence of phase slip (PS) centers at superconductor (S) - normal metal (N) interfaces [29]. Then, the onset of the Ohmic behavior in I-V characteristics would correspond to suppression of the non-equilibrium superconducting regime or the transition to the normal state. Figure 2(a) also demonstrates the appearance of voltage plateaus in I-V curves. These plateaus develop at two voltage levels, viz., at the normal state voltage V_N and at $V_P \approx V_N/2$. The similar plateau at $V_P \approx V_N/2$ has been reported for low- T_C superconducting nanowires in non-hysteretic out-of-equilibrium dissipative regime [30].

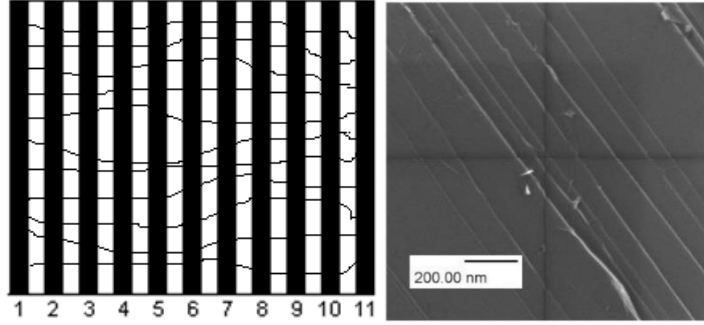


Fig.1. Left: The geometry of the experiment. The numbers correspond to eleven silver epoxy electrodes patterned with a distance $d = 0.2$ mm on cleaved surface of HOPG sample. Thin curved lines are schematically drawn line defects. Right: Scanning electron microscope (SEM) image of the HOPG sample demonstrating large scale nearly parallel line defects [25].

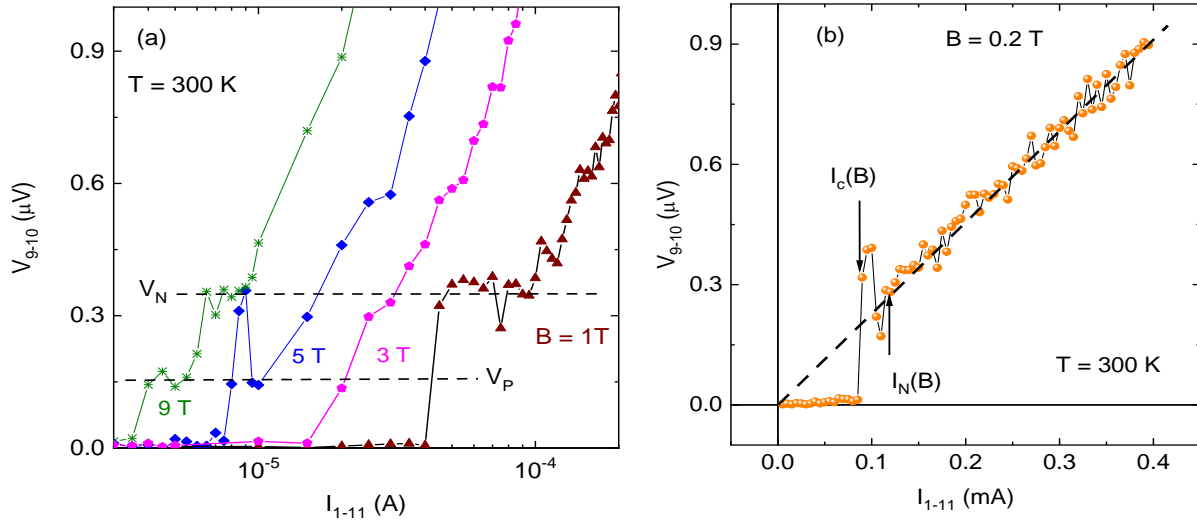


Fig. 2. Current-voltage (I-V) characteristics measured at $T = 300$ K for various applied magnetic fields. (a) Semilogarithmic plot of I-V curves obtained for selected applied magnetic fields. $V_N = 0.36$ $\mu\text{V} \approx 2\text{V}$ (see text). (b) I-V curve on a linear scale obtained for $B = 0.2$ T; dashed line corresponds to the Ohmic law. $I_C(T,B)$ and $I_N(T,B)$ are currents corresponding to transitions to superconducting and normal state, respectively.

The I-V characteristics measurements reveal a qualitatively different $I_C(T,B)$ behavior below and above the “crossover” field $B_x \approx 35 \pm 5$ mT, that separates $dI_C/dT < 0$ and $dI_C/dT > 0$

behavior for $B < B_x$ and $B > B_x$, respectively. Figures 3 and 4 demonstrate this behavior for the I-V curves measured for $B = 0$, see Fig. 3, and $B = 9$ T, see Fig. 4 for some selected temperatures.

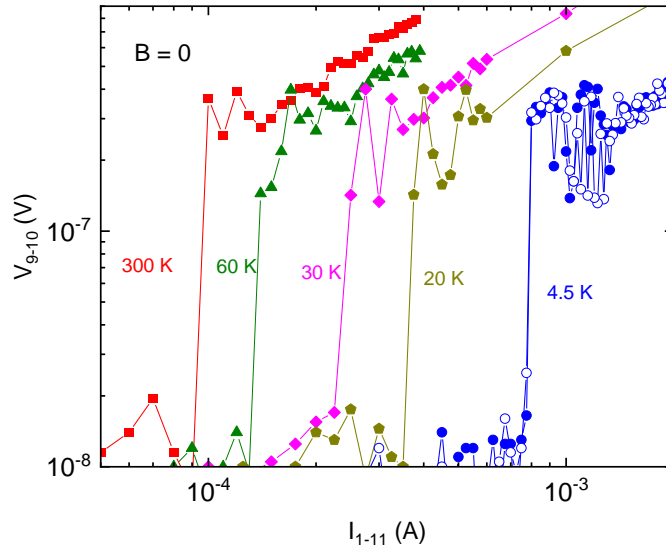


Fig. 3. Selected I-V characteristics, measured at $B = 0$ and $4.5 \text{ K} \leq T \leq 300 \text{ K}$, demonstrate decrease of the critical current $I_c(T)$ with the temperature increasing. Measurements at $T = 4.5 \text{ K}$ were performed for both increasing (\bullet) and decreasing (\circ) current, testifying the reversible character of I-V curves.

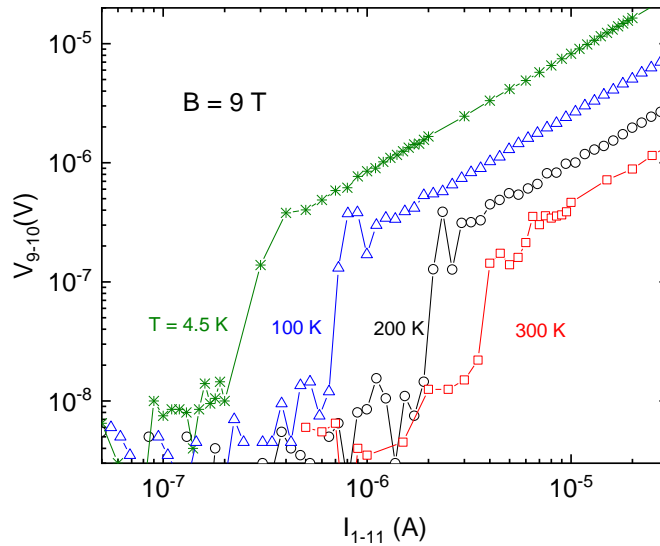


Fig. 4. I-V characteristics, measured for $B = 9 \text{ T}$ and $4.5 \text{ K} \leq T \leq 300 \text{ K}$ demonstrate the increase of the critical current $I_c(T)$ with the temperature increasing.

Figure 5 summarizes the results of the $I_c(T, B)$ measurements. The existence of the “crossover” field $B_x \approx 35$ mT that separates the “normal-like” (typical for most superconductors) $dI_c/dT < 0$ at $B < B_x$ behavior, and “anomalous” $dI_c/dT > 0$ at $B > B_x$ behavior is clear. To better visualize the “anomalous” $I_c(T, B)$ behavior, we plot in the inset in Fig. 5, $I_c(T, B)$ for a few selected fields. Note, that the $dI_c/dT > 0$ behavior is well known for type-II superconductors, and takes place either in the vicinity of the upper critical field $B_{c2}(T)$ or just below the Abrikosov vortex lattice melting phase transition [31], but is usually seen only within a narrow interval of B and T . In our case, e.g. $I_c(T, 9$ T) rises over about 10 times as the temperature increases from 4.5 (20) K to 300 K (see the inset in Fig. 5). At the same time, a broad maximum in $I_c(T)$ and $dI_c/dT > 0$ for $T \ll T_C$ was reported for various granular or/and inhomogeneous superconductors, such as, for instance, $\text{BaPb}_{0.75}\text{Bi}_{0.25}\text{O}_3$ granular superconductor [32], $\text{Sn-SnO}_x\text{-Sn}$ tunnel Josephson junctions (JJ) [33], and Zn-Sb inhomogeneous alloys [34], and attributed to a (quasi)-reentrance (due to different mechanisms) of the superconducting transition in the Josephson medium.

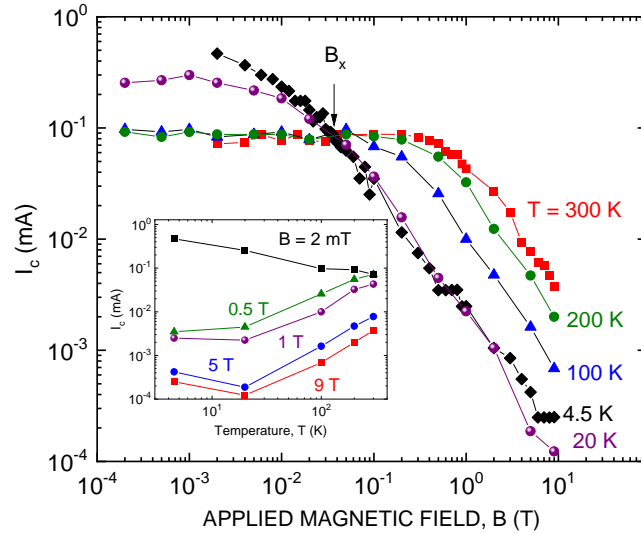


Fig. 5. Magnetic field dependencies of the critical current $I_c(B, T)$ extracted from I-V isotherms. The “crossover” field $B_x \approx 35$ mT separates $dI_c/dT < 0$ ($B < B_x$) and $dI_c/dT > 0$ ($B > B_x$) behaviors. Inset illustrates $I_c(T)$ obtained for some selected magnetic fields from the main figure.

In Fig. 6 we plot the normalized critical current $I_c(T)/I_c(T=T_{\max})$ vs. T/T_{\max} for $\text{BaPb}_{0.75}\text{Bi}_{0.25}\text{O}_3$ [32], Zn-Sb [34] together with our data for $I_c(T, B)$ obtained for $B = 1$ T $\gg B_x$, where T_{\max} corresponds to the maximal value of I_c . As seen from Fig. 6, $I_c(T)$ dependencies are quite similar for both $\text{BaPb}_{0.75}\text{Bi}_{0.25}\text{O}_3$ [32] and Zn-Sb [34] superconductors. For instance, one gets the ratio $T_{\max}/T_C \approx 0.7$ for both superconductors. Assuming that $I_c(T, B = 1$ T) in our case reaches maximum at $T_{\max} \geq 300$ K, the highest measuring temperature, one gets surprisingly good matching between our and the literature data (see Fig. 6) suggesting that the JJ array-like medium can be indeed behind of the $I_c(T)$ behavior in all these materials. We have also found, that the $I_c(T,$

B) behavior can be fully described by using the temperature and magnetic field dependences of the normal state resistance $R_N(T, B)$.

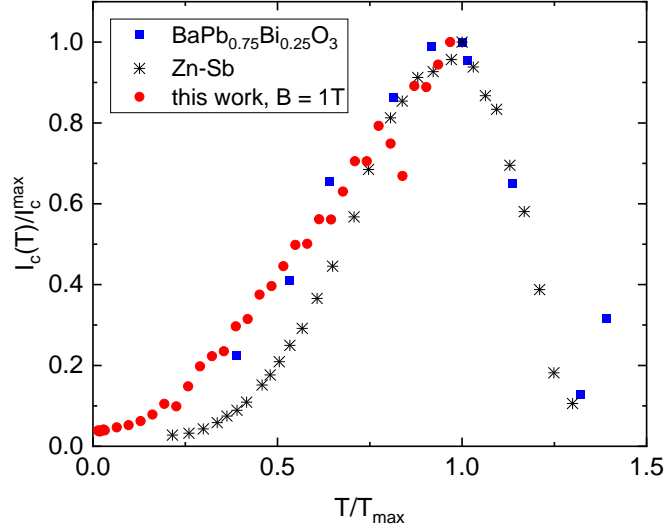


Fig. 6. Reduced $I_c(T)$ vs. reduced T for $\text{BaPb}_{0.75}\text{Bi}_{0.25}\text{O}_3$ [32], Zn-Sb [34], and graphite (this work). $I_c(T)$ reaches the maximum value I_c^{max} at $T = T_{\text{max}}$. Our data for $I_c(T, B = 1 \text{ T})$ are the same as in Fig. 7(a) assuming $T_{\text{max}} = 300 \text{ K}$.

Figure 7(a) presents $I_c(T)$ for $B = 0$ and $B = 1 \text{ T}$ for $4.5 \text{ K} \leq T \leq 300 \text{ K}$. The experimental data can be nicely fitted by solid lines obtained from the equation $I_c(T, B) = V_c/R_N(T, B)$, where $V_c = 0.2 \mu\text{V}$. The resistance $R_N(T, B)$ temperature dependences measured for $B = 0$ and $B = 1 \text{ T}$, are shown in Fig. 7(b). One sees that the crossover from the “conventional”, $dI_c/dT < 0$ for $B = 0$, to “anomalous” $dI_c/dT > 0$ for $B = 1 \text{ T}$ behavior is governed by the field-induced transformation from the metallic-like $dR_N/dT > 0$ at $B < B_x$ to the insulator-like $dR_N/dT < 0$ at $B > B_x$ resistance behavior.

Figure 8 illustrates the universality of the equation $I_c R_N = V_c$. One sees that I_c vs. R_N^{-1} dependencies obtained for various T and B collapse on a single line $I_c = V_c \cdot R_N^{-1}$ with $V_c = 0.2 \mu\text{V}$, spanning about 4 orders of magnitude in both $I_c(T, B)$ and $R_N(T, B)$ dependences. This kind of relationship for the maximum critical current given by $I_c = (\pi\Delta/2eR_N) \cdot \tanh(\Delta/2k_B T)$ emerges in the celebrated Ambegaokar-Baratoff (AB) description of the superconductor-insulator-superconductor (SIS) of the Josephson junction (JJ) [35]. Then, $I_c(T = 0) = \pi\Delta(0)/2eR_N$ and $I_c(T_c/2) \sim 0.9I_c(0)$, where $\Delta(0)$ is the magnitude of the superconducting gap at zero temperature, and R_N is the JJ resistance just above T_c . However, taking the experimental values of $I_c = 9 \cdot 10^{-4} \text{ A}$ and $R_N = 2 \cdot 10^{-4} \Omega$ for $T = 4.5 \text{ K}$ and $B = 0$, one gets $\Delta(0) \sim 10^{-7} \text{ eV}$ which is by many orders of magnitude much too small to account for the experimental results, unless some additional assumptions on the strong depression of the $I_c R_N$ product are considered, see e.g. [36, 37].

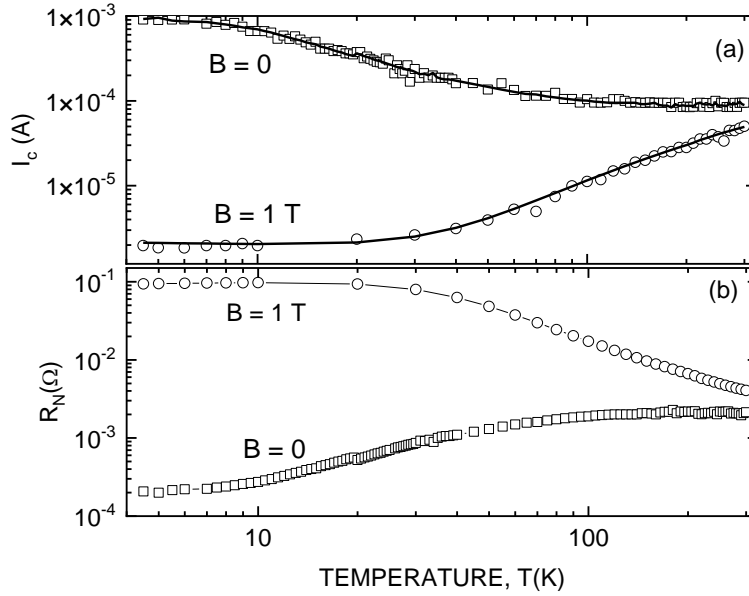


Fig. 7. (a) $I_c(T, B)$ obtained from I-V characteristics for $4.5 \text{ K} \leq T \leq 300 \text{ K}$ at $B = 0$ and $B = 1 \text{ T}$. Solid lines are obtained from the equation $I_c = V_c/R_N(T, B)$, $V_c = 0.2 \mu\text{V}$, and $R_N(T, B)$ is the normal state resistance; (b) $R_N(T, B)$ for $B = 0$ and $B = 1 \text{ T}$ obtained for $I > I_c(T, B)$ in the Ohmic regime.

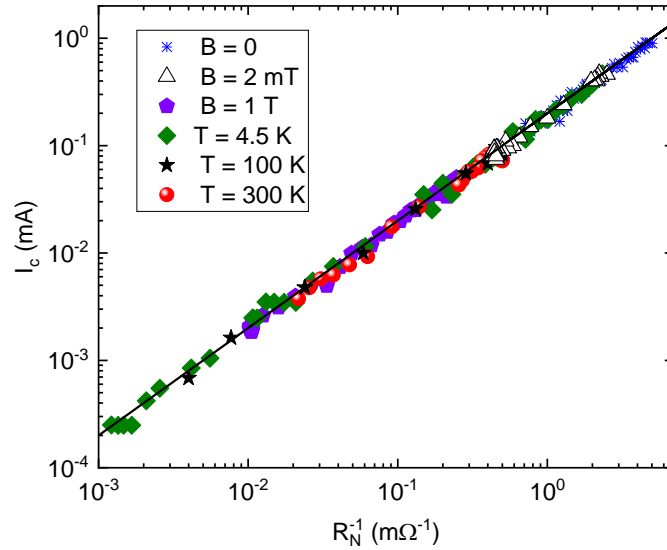


Fig. 8. $I_c(T, B)$ vs. $R_N(T, B)$ obtained from I-V characteristics measured at fixed temperature ($T = 4.5, 100, \text{ and } 300 \text{ K}$) or magnetic field ($B = 0, 2 \text{ mT}, \text{ and } 1 \text{ T}$). The solid line corresponds to the equation $I_c = V_c \cdot R_N^{-1}$ with $V_c = 0.2 \mu\text{V}$.

To better characterize the superconducting transition, we perform the resistance measurements as a function of temperature, magnetic field and applied current. Figure 9 (a, b) presents the voltage $V(T)$ and the resistance $R(T) = V(T)/I$ records for various measuring currents and $B = 0$. We see that the superconducting transition temperature $T_c(I)$ decreases as the current increases, and that for $I \geq 2$ mA no transition is seen down to $T = 4.5$ K. Fig. 9 (a, b) also demonstrates several important features: (i) the two-step transition towards the superconducting state, (ii) the voltage plateaus at $V_P = V_N/2$ within the certain temperature interval $\Delta T(I)$, and (iii) stochastic switching between the superconducting state ($V = 0$), the voltage plateau with $V = V_P$ and normal state. Figure 9 (b) provides the evidence for the Ohmic resistance $R(T)$ for $I \geq 2$ mA. The inset in Fig. 9(b) presenting the $I_c(T)$ together with the data of Fig.7(a) for $I_c(T, B = 0)$ shows a good agreement of both dependences.

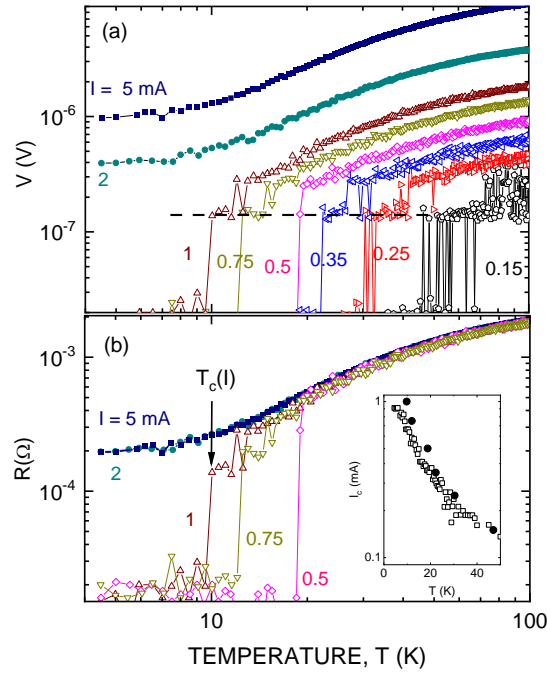


Fig. 9. (a) $V = V_{9-10}(T, B = 0)$ measured for various currents $I = I_{1-11}$ at $B = 0$; dashed line corresponds to the voltage level $V = 0.15 \mu\text{V}$; (b) $R(T) = V(T)/I$ obtained from (a) for selected currents; the inset presents $I_c(T)$ (\bullet) together with the data of Fig.7(a) (\square) for $I_c(T, B = 0)$.

Figure 10 presents the resistance $R(T, B)$ for various applied fields $0 \leq B \leq 40$ mT and the current $I = 0.5$ mA, which is slightly below $I_c(4.5 \text{ K}, B = 0)$, together with $R(T, B)$ obtained for $I = 5 \text{ mA} > I_c$. The curves $R(T, B)$ obtained for $B = 0, 0.5$ mT, and 1 mT demonstrate the sharp superconducting transitions, as well as the stochastic switching between the superconducting state, the “intermediate” state possessing $R \approx R_N/2$, and the normal state. Figure 10 further illustrates

that the resistance switching is not observable at temperatures below ≈ 18.5 K for $B = 0$, as well as at $T \leq 10$ K for $B = 0.5$ mT, and at $T \leq 8.5$ K for $B = 1$ mT, revealing the magnetic field effect on stability of both the superconducting and the resistive states. For $B \geq 10$ mT, the sample is in the normal Ohmic state, as evident from the resistance measurements at $I = 5$ mA shown by solid lines. Further increase of B results in the upturn, $dR/dT < 0$, behavior for $T < T_{\min}(B = 30 \text{ mT}) = 37 \pm 1$ K, and $T < T_{\min}(B = 40 \text{ mT}) = 45 \pm 1$ K. The results shown in Fig. 10 resemble the magnetic-field-driven superconductor-insulator transition (SIT), observed in two-dimensional (2D) Josephson junction arrays (JJA) [38] and superconducting films [39], as well as in arrays of 1D superconducting wires [40]. It worth noting that graphite, both HOPG and single crystals with no signature for the global superconductivity, demonstrate the field-induced metal-insulator (MIT) - like behavior, identical to what is shown in Fig. 10 [41].

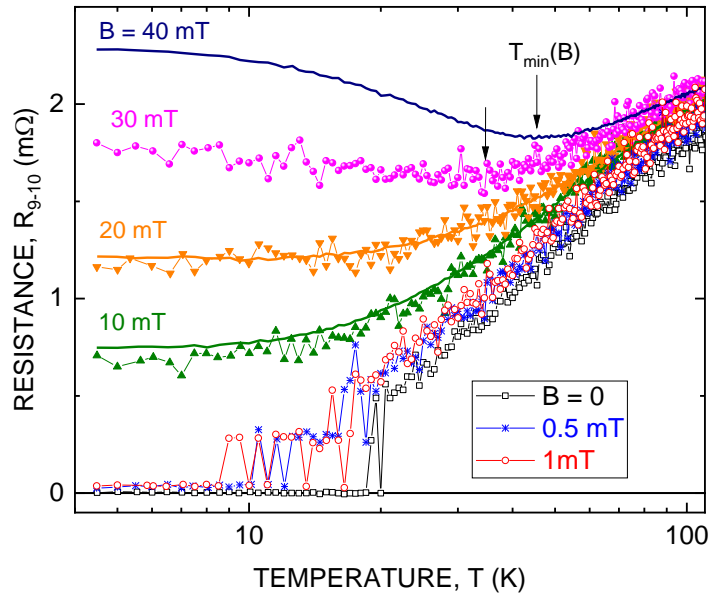


Fig.10. $R \equiv R_{9-10}(T, B)$ measured with $I_{1-11} = 0.5$ mA (symbols) for various magnetic fields $0 \leq B \leq 40$ mT. Solid lines are $R(T, B)$ measured for $I = 5$ mA $> I_c$. Arrows mark $T_{\min}(B)$ corresponding to the minima in $R(T, B)$ curves.

The voltage/resistance plateaus observed in our I-V and $R(T, B, I)$ measurements, as well as the switching between higher and lower voltage/resistance states are similar to the phenomena observed in other superconductors, such as, e. g., Zn [30] and Al [42] nanowires, $\text{Mo}_x\text{Si}_{1-x}$ films [43], Nb/Ru/ Sr_2RuO_4 junctions [44] and $\text{YBa}_2\text{Cu}_3\text{O}_{7-\delta}$ films with line defects [45] Discussion of these results is out of the scope of the present Letter, and will be reported elsewhere.

Now, we briefly discuss the possible origin of the global RTSC in graphite samples with line defects. Experimental evidences accumulated during the past two decades indicate that both SC- and competing ferromagnetic (FM) - like orders in graphite, observed even above the room temperature, are related to structural defects [14, 46, 47]. It is therefore important the formation of the LDs representing a rich morphology of the disordered graphitic structures such as corrugations (wrinkles) [48, 49], steps of the height $h_0 \leq h \leq 5h_0$, where $h_0 = 3.35 \text{ \AA}$ is the distance between neighboring graphene planes in Bernal graphite, folded multi-layer graphene ridges and strands [14, 46, 50, 51]. Because of the structural disorder, the resistance of LDs in the normal state is insulating- or “bad metal” - like ($dR/dT < 0$) [25].

The fact that the relation between the critical current $I_C(T, B)$ and the normal state resistance $R_N(T, B)$ resembles that of the JJ, suggests that the LDs can be viewed as “chains” of the superconducting islands or “granules” hosting the local SC order at $T > 300 \text{ K}$. At the same time, because $R_N(T, B)$ is the resistance of the bulk graphite, the relation $I_C(T, B) \sim 1/R_N(T, B)$ indicates the crucial role of the non-superconducting bulk graphite “substrate” that controls establishing of the global phase coherence between the SC islands by suppressing the phase slips. This picture is in line with the old proposal by Emery and Kivelson [52], and its development in [53] demonstrating that the metallic layer weakly coupled to “pairing layer” with the absent of the phase stiffness, stabilizes superconductivity and may drive the superconducting transition temperature up to $T_C \approx \Delta_0/2$, where Δ_0 is the preexisting value of the gap in the “pairing layer.” In our case, this Δ_0 is the zero-temperature gap corresponding to the local “intragrain” superconductivity. Taking $T_c \sim 500 \text{ K}$ obtained from superconducting magnetization $M(H)$ hysteresis loop measurements [14] and BCS result $2\Delta_0/k_B T_c = 3.52$, one arrives at $\Delta_0 \sim 80 \text{ meV}$ (see Ref. [54] for the most recent report on local superconductivity in graphite with $T_c \geq 500 \text{ K}$). It is interesting to note, that scanning tunneling spectroscopy measurements performed on the graphite surface at $T = 4.2 \text{ K}$ revealed a gap in electronic spectrum $\sim 50 - 100 \text{ meV}$ [55]. As it was emphasized in [56], such SC-like gap occurs only in structurally disordered surface regions.

We are aware of at least two experiments where the dissipative coupling between a “conducting layer” and JJ array [57] or 2D films [58] triggers the finite temperature superconductivity. In both cases the capacitive coupling, that cannot be excluded in our case as well, is behind the phase fluctuations damping. To reveal whether we have capacitive or electron tunneling dissipative coupling further experiments are required.

Another characteristic feature of structurally disordered graphitic patches was obtained from the angle-resolved photoemission spectroscopy (ARPES) measurements performed on cleaved HOPG [59] and graphite single crystals [60]. These studies revealed the presence of weakly dispersive electron band situated within $\sim 50 \text{ meV}$ below the Fermi energy (E_F) with the electron concentration $n_e \sim 10^{20} \text{ cm}^{-3}$ and the effective mass $m_e^* \approx 0.5m_e$ [57]. The enhanced density of states, being consistent with the presence of shallow electronic bands, has been also detected at graphitic edge steps and LDs in STM experiments [46, 61, 62].

Regarding the origin of a high pairing energy in LDs, let us mention first two theoretical results [63, 64] based on the resonating valence bonds (RVB) physics that predict the mean field $T_c^{MF} \leq 4 \cdot 10^3 \text{ K}$ [63] and $T_c \approx 600 \text{ K}$, as estimated from the weak coupling BCS theory [64], for optimally doped graphene. Disorder-induced self-doping [59] and charge transfer between the defects and the bulk graphite is the possibility to meet the HTSC conditions. The high energy scale for pairing has been also proposed for graphene fragments where Monte Carlo simulations revealed the emergence of the quantum spin liquid [65] with the spin gap $\Delta_s = 0.7 \text{ eV}$. Then,

considering Δ_s being the pairing energy, as in a short-range RVB model [66], the authors of Ref. [65] suggest the emergence of HTSC in graphene under doping.

Another possibility of obtaining high pairing temperature in layered materials containing local deformations and structural disorder, and experiencing the transition from superconducting to insulating-like behavior as shown in Fig. 10 is the (pseudo)monopole pairing mechanism [67]. The energy scale defining the pairing energy $\Delta_0 \approx \hbar^2/m^*d^2$, where m^* is the effective mass of the paired electrons and d is the distance between the layers hosting each of electrons. Taking $m^* = 0.5m_e$ and $d = 4 \text{ \AA}$, as in LD, one gets $\Delta_0 \approx 0.7 \text{ eV}$. The hint that layered structures can harbor (pseudo)monopoles can be taken from the results of [68] demonstrating that the monopole may appear as an image of an electron near the surface of the topological insulator. The experiment by A. Uri et al. [69] using the graphene layer as the surface creating this image confirmed the emergence of the (pseudo)monopole. The reliable conclusions and revealing the nature of the pairing mechanism requires more detailed and careful experimental and theoretical work, which will be the subject of forthcoming publications.

This work was supported by FAPESP, CNPq (Brazilian agencies) and by Terra Quantum AG.

References

- [1] H. Kamerlingh Onnes, Commun. Phys. Lab. Univ. Leiden. Suppl. 29 (Nov. 1911).
- [2] J. G. Bednorz and K. A. Müller, Z. Phys. B **64**, 189 (1986).
- [3] M. K. Wu et al., Phys. Rev. Lett. **58**, 908 (1987).
- [4] A. Schilling et al., Nature **363**, 56 (1993).
- [5] L. Gao et al., Phys. Rev. B **50**, 4260 (1994).
- [6] K. Tanigaki, Nature **352**, 222 (1991).
- [7] J. Nagamatsu et al. Nature **410**, 63 (2001).
- [8] G. Gao et al, Materials Today Physics **21**, 100546 (2021).
- [9] N. B. Hannay et al., Phys. Rev. Lett. **14**, 225 (1965).
- [10] T. E. Weller, et al., Nature Physics **1**, 39 (2005).
- [11] N. Emery et al., Phys. Rev. Lett. **95**, 087003 (2005).
- [12] K. Antonowicz, Nature **247**, 358 (1974).
- [13] K. Antonowicz, Phys. Status Solidi A **28**, 497 (1975).
- [14] Y. Kopelevich et al., J. Low Temp. Phys. **119**, 691 (2000).
- [15] R. R. da Silva et al. Phys. Rev. Lett. **87**, 14700 (2001).
- [16] N. P. Yang et al., Chin. Phys. Lett. **18**, 1648 (2001).
- [17] Y. Kawashima, AIP Advances **3**, 052132 (2013).
- [18] Y. Kopelevich et al., Physica C **514**, 237 (2015).
- [19] I. Felner et al., Phys. Rev. B **79**, 233409 (2009).
- [20] S. Moehlecke, Y. Kopelevich, and M. B. Maple, Phys. Rev. B **69**, 134519 (2004).
- [21] P. J. F. Harris et al., Phil. Mag. Lett. **80**, 381 (2000).
- [22] A. Ballestar et al., New J. Phys. **15**, 023024 (2013).
- [23] A. Ballestar et al., Carbon **72**, 312 (2014).
- [24] E Precker et al., New J. Phys. **18**, 113041 (2016).
- [25] Y. Kopelevich et al., J. Phys.: Condens. Matter **25**, 466004 (2013).

- [26] H. J. Mamin et al. Phys. Rev. B **29**, 3881 (1984).
- [27] R. Wortis, and D. A. Huse, Phys. Rev. B **54**, 12413 (1996).
- [28] J.H.S. Torres et al. Solid State Commun. **125**, 11 (2003).
- [29] M. Park et al., Phys. Rev. Lett. **75**, 3740 (1995), and refs. therein.
- [30] Y. Chen et al., Nat. Phys. **10**, 567 (2014).
- [31] W. Kwok et al., Phys. Rev. Lett. **73**, 2614 (1994).
- [32] T. H. Lin et al., Phys. Rev. B **29**, 1493 (1984).
- [33] H. Akoh et al., Phys. Rev. B **33**, 2038 (1986).
- [34] V. M. Gantmakher et al., JETP Lett. **59**, 446 (1994).
- [35] V. Ambegaokar and A. Baratoff, Phys. Rev. Lett. **10**, 486 (1963).
- [36] M. Yu. Kupriyanov and K. K. Likharev, IEEE Trans. on Magn. **27**, 2460 (1991).
- [37] J. K. Freericks, B. K. Nikolic, and P. Miller, Phys. Rev. B **64**, 054511 (2001).
- [38] H. S. J. van der Zant et al, PRL **69**, 2971 (1992); PRB **54**, 10081 (1996).
- [39] N. Mason and A. Kapitulnik, Phys. Rev. Lett. **82**, 5341 (1999).
- [40] D. B. Haviland et al., Journal of Low Temp. Phys. **118**, 733 (2000).
- [41] Y. Kopelevich et. al., in: Adv. Solid State Phys. **43**, 207 (2003), ed. by B. Kramer; Springer-Verlag Berlin Heidelberg 2003), and Phys. Rev. Lett. **90**, 156402 (2003).
- [42] M. Singh and M. H. W. Chan, Phys. Rev. B **88**, 064511 (2013).
- [43] S. Okuma et al., Phys. Rev. B **76**, 224521 (2007).
- [44] M. S. Anwar et al., Sci. Rep. **3**, 2480 (2013).
- [45] A. Jukna, Materials **15**, 4260 (2022).
- [46] P. Esquinazi et al., Phys. Rev. B **66**, 024429 (2002).
- [47] J. Cervenka et al., Nat. Phys. **5**, 840 (2009).
- [48] B. C. Camargo et al., Appl. Phys. Lett. **108**, 031604 (2016).
- [49] L. Meng et al., Carbon **156**, 24 (2020).
- [50] T. L. Makarova and K.H. Han, Phys. Status Solidi b **244**, 4138 (2007).
- [51] H. Chang and A. J. Bard, Langmuir, **7**, 1143 (1991).
- [52] V. J. Emery and S. A. Kivelson, Nature **374**, 434 (1995). Phys. Rev. Lett. **74**, 3253 (1995).
- [53] E. Berg et al., Phys. Rev. B **78**, 094509 (2008).
- [54] R. Rousset-Zenou et al., arXiv:2207.09149.
- [55] N. Agrait et al., Ultramicroscopy **42-44**, 177 (1992).
- [56] Y. Kopelevich and P. Esquinazi, J. Low Temp. Phys. **146**, 626 (2007).
- [57] A. J. Rimberg et al., Phys. Rev. Lett. **78**, 2632 (1997).
- [58] N. Mason and A. Kapitulnik, Phys. Rev. B **65**, 220505 (2002).
- [59] S. Y. Zhou et al., Nat. Phys. **2**, 595 (2006).
- [60] K. Sugawara et al., Phys. Rev. B **73**, 045124 (2006).
- [61] Y. Niimi et al., Phys. Rev. B **73**, 085421 (2006).
- [62] L. Feng et al., APL **101**, 113113 (2012).
- [63] A. M. Black-Schaffer and S. Doniach, Phys. Rev. B **75**, 134512 (2007).
- [64] S. Pathak et al., Phys. Rev. B **81**, 085431 (2010).
- [65] Z. Y. Meng et al., Nature **464**, 847 (2010).
- [66] S. A. Kivelson et al., Phys. Rev. B **35**, 8865 (1987).
- [67] M. C. Diamantini, C. A. Trugenberger, and V. M. Vinokur, arXiv:2102.08652.
- [68] X.-L. Qi et al., Science **323**, 1184 (2009).
- [69] A. Uri et al., Nat. Phys. **16**, 164 (2020).